Comparative study of tip cross-sections for efficient galloping energy harvesting

Yaowen Yang, Liya Zhao, and Lihua Tang

Related Articles

Additional information on Appl. Phys. Lett.

Comparative study of tip cross-sections for efficient galloping energy harvesting

Yaowen Yang,[a)] Liya Zhao, and Lihua Tang
School of Civil and Environmental Engineering, Nanyang Technological University, 50 Nanyang Avenue, Singapore 639798

This letter presents a comparative study of different tip cross-sections for small scale wind energy harvesting based on galloping phenomenon. A prototype device is fabricated with a piezoelectric cantilever and a tip body with various cross-section profiles (square, rectangle, triangle, and D-shape) and tested in a wind tunnel. Experimental results demonstrate the superiority of the square-sectioned tip for the low cut-in wind speed of 2.5 m/s and the high peak power of 8.4 mW. An analytical model is established and verified by the experimental results. It is recommended that the square section should be used for small wind galloping energy harvesters. © 2013 American Institute of Physics. [http://dx.doi.org/10.1063/1.4792737]

Development of self-powered sensors by harvesting ambient energy has been researched explosively in the past years due to the inconvenience and high cost of replacement of batteries. Many studies have been conducted on vibration-based energy harvesting.[1–5] However, small wind energy harvesting has received less attention. Flow-induced vibrations due to vortex shedding, galloping, flutter, and wake galloping can be harnessed using piezoelectric energy harvesters (PEHs).[6–22] Various designs of PEH have been reported, including a bio-inspired cross-flow piezo-leaf,[6] a flapping wing with airfoil section,[7–10] a T-shaped piezoelectric cantilever,[11] a self-sustained MEMS wind sensor implementing micro PEH for scavenging turbulence-induced vibrations,[12] a cantilever with a windward cylinder attached to the tip operating through vortex-induced vibrations,[13–15] and some other designs.[16–18] Translational galloping is a self-excited aeroelastic phenomenon, giving rise to transverse oscillations normal to the direction of wind flows in structures with weak damping when wind velocity exceeds a critical value. It is a better choice to obtain structural vibrations for energy harvesting purpose compared to the vortex-induced vibrations and flutter, for its advantage of large vibration amplitude and the ability of oscillating in infinite range of wind velocities. Barrero-Gil *et al.*[19] theoretically analyzed the potential use of transverse galloping to obtain energy using a single-degree-of-freedom (SDOF) model. Different galloping energy harvesters consisting of cantilevers with attached prisms of triangular and D-shape cross-sections have been reported by Sirohi and Mahadik.[20,21] Abdelkefi *et al.* theoretically analyzed the influence of load resistance and bluff body cross-section geometry on the onset of galloping and harvested power.[22] However, no experimental comparative study has been reported in the literature.

This letter presents an experimental study on the influence of cross-section geometries (square, rectangles with distinct aspect ratios, equilateral triangle, and D-section) of bluff bodies on galloping piezoelectric energy harvesting in the laminar flow condition. The flow condition is kept the same for all harvesters to ensure fair comparison. A lumped parameter single-degree-of-freedom (1DOF) model integrating electromechanical and aerodynamic formulations is also established and validated.

The proposed galloping energy harvester consists of a piezoelectric cantilever beam clamped at one end, and connected to a rigid prism with a specific cross section at the free end (Fig. 1(a)). Translational galloping was first analyzed by Den Hartog.[23] The simplified SDOF model comprises a bluff body M mounted on a spring K and a damping C as shown in Fig. 1(b). Wind U flows from the right to the left, with the angle of attack α. The aerodynamic force F_z acting on the bluff body causes it to oscillate in the z direction. A criterion for galloping is identified as $\partial C_{Fz}/\partial \alpha > 0$, where C_{Fz} is the aerodynamic force coefficient.[24]

Figure 2(a) shows the schematic of the proposed energy harvester. The fabricated prototype device and the experimental setup in the wind tunnel are shown in Fig. 2(b). The joint of the connection between the beam and the tip is detachable. The dimensions of the aluminum cantilever are $L_b = 150$ mm, $B_b = 30$ mm, and $t_b = 0.6$ mm. Two piezoelectric sheets (DuraAct P-876.A12 from Physik Instrumente) are attached to the root of the cantilever beam on both sides, and connected in parallel. Each piezoelectric sheet has a length of 61 mm, a width of 30 mm, a thickness of 0.5 mm, and a capacitance of 90 nF. The cantilever and each piezoelectric sheet weigh 7.29 g and 3.5 g, respectively. Considering different values of $\partial C_{Fz}/\partial \alpha$ of various cross sections[24] of the tip body, five cross sections are chosen for comparison, including square, equilateral triangle, two rectangles with different aspect ratios, and D-section. The five tip bodies have equal length of 150 mm and equal area of wind exposure as 40×150 mm^2. Dimensions of the tip cross sections are shown in Table I. For a fair comparison, the weights of the five tip bodies are all adjusted to 26.8 g by attaching various steel masses onto their inner surfaces to achieve a constant fundamental frequency for the harvester with different tip bodies.

The analytical model of the proposed harvester should take into account the electromechanical coupling effect, as

---

[a)]Author to whom correspondence should be addressed. Electronic mail: cywyang@ntu.edu.sg.
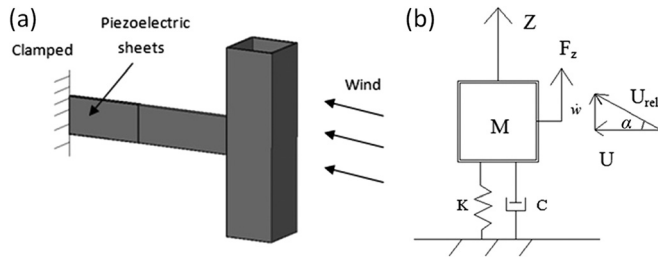
FIG. 1. (a) Proposed galloping PEH and (b) schematic of a bluff body subjected to wind flows.

well as the interaction between the wind flow and the tip body. A coupled SDOF model is developed to simulate the electro-fluid-structural coupling behavior. The governing equations are written as

$$
\begin{cases}
M_{eff}\ddot{w} + C\dot{w} + Kw + \Theta V = F_Z \\
\dfrac{V}{R_L} + C_P\dot{V} - \Theta\dot{w} = 0
\end{cases}
\tag{1}
$$

where w, C, and K are the tip displacement in the direction normal to the wind flow, the damping coefficient, and the stiffness of the harvester, respectively; V and R_L are the generated voltage and applied load resistance, respectively; C_P is the total capacitance of the piezoelectric sheets in parallel connection; Θ is the electromechanical coupling coefficient; and M_{eff} is the effective mass expressed by $M_{eff} = (33/140)M_b + M_{tip}$ with M_b and M_{tip} being the mass of the cantilever and the tip body, respectively. The coupling coefficient Θ is obtained as

$$
\Theta = \sqrt{(\omega_{noc}{}^2 - \omega_{nsc}{}^2)M_{eff}C_P}
\tag{2}
$$

where ω_{noc} and ω_{nsc} are the fundamental natural frequencies of the harvester for the open circuit and short circuit conditions, respectively. The aerodynamic model established here is based on the quasi-steady hypothesis.[24] The aerodynamic force is given as

$$
F_Z = \frac{1}{2}\rho_a h L_{tip} U^2 C_{F_Z}
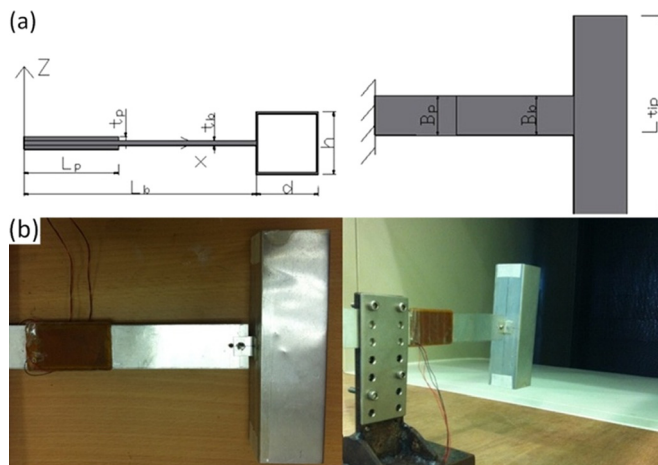\tag{3}
$$

FIG. 2. (a) Top and side views of the proposed galloping energy harvester and (b) experimental setup.

TABLE I. Dimensions of tip cross sections.

Section shape	□ ←	□ ←	□ ←	◁ ←	◖ ←
Dimension h × d (mm)	40 × 40	40 × 60	40 × 26.7	40 (side)	40 (dia.)

where ρ_a, h, L_{tip}, and U are air density, frontal dimension facing the wind flow (Fig. 2(a)), length of the tip body, and wind velocity, respectively. C_{F_Z} can be expressed as a polynomial function of the angle of attack α

$$
\begin{cases}
C_{F_Z} = \displaystyle\sum_{i=1}^{m} A_i(\alpha)^i + \sum_{j=2}^{k} A_j(\alpha)^j\,\frac{\dot{w}}{|\dot{w}|} \\
\alpha = \dfrac{\dot{w}}{U} + w'(L_b)
\end{cases}
\tag{4}
$$

where $\dot{w}$ is the vibration velocity of the tip body; A_i and A_j are the empirical coefficients; and $w'(L_b)$ denotes the rotation angle of the beam at the free end due to the translational motion. The first sum in the expression of C_{F_Z} involves odd integers (i, m) and the second involves even integers (j, k).

The root of the beam is clamped using a metal support during the wind tunnel test. Wind velocity is measured using a pitot tube and a manometer. Voltage data are acquired through the NI 9229 DAQ module. The average output power is calculated by $P = V_{RMS}{}^2/R_L$, where V_{RMS} is the root mean square (RMS) voltage across R_L.

Figure 3(a) shows the output power measured over a range of load resistances at different wind velocities for the proposed harvester with a square-sectioned tip. The optimal load resistance is around 105 kΩ and hardly changes with the wind velocity (in our testing range). Here, the optimal load resistance refers to the one when the output power is the maximum. For galloping energy harvesters with different tip bodies, the optimal R_L is obtained at a specific wind velocity and applied to all wind velocities.

Figure 3(b) shows the measured output power versus load resistance at a wind velocity of 6 m/s for the five cross sections. It is observed that the optimal R_L for the five cross sections are almost the same, which are all around 105 kΩ. This is reasonable. The oscillation frequency due to galloping is always consistent with the fundamental frequency of the harvester,[24] which is equal for the five harvesters since the tip masses are the same and the axial force on the beam due to wind is negligible. Hence, equal optimal R_L is achieved, which can be approximated by $R_L = 1/\omega_n C_p$.

The measured voltage and output power at different wind velocities with optimal R_L are plotted in Figs. 3(c) and 3(d), respectively. It is obvious that the square section generates the largest voltage and power, with a peak output power of 8.4 mW measured at 8 m/s, which is also higher than the peak power achieved in the literature (e.g., 4 mW in Ref. 11, 2.2 mW in Ref. 7, 1.14 mW in Ref. 21). Moreover, the square section starts to oscillate at a wind velocity of 2.5 m/s, which is lower than the other harvesters in our test and other previously reported ones (e.g., 4 m/s in Ref. 11, 8 mph (3.576 m/s) in Ref. 20). This could be attributed to the largest value of $\partial C_{F_Z}/\partial \alpha$ for the square section according to the criterion of galloping instability.[24] Power outputs for the
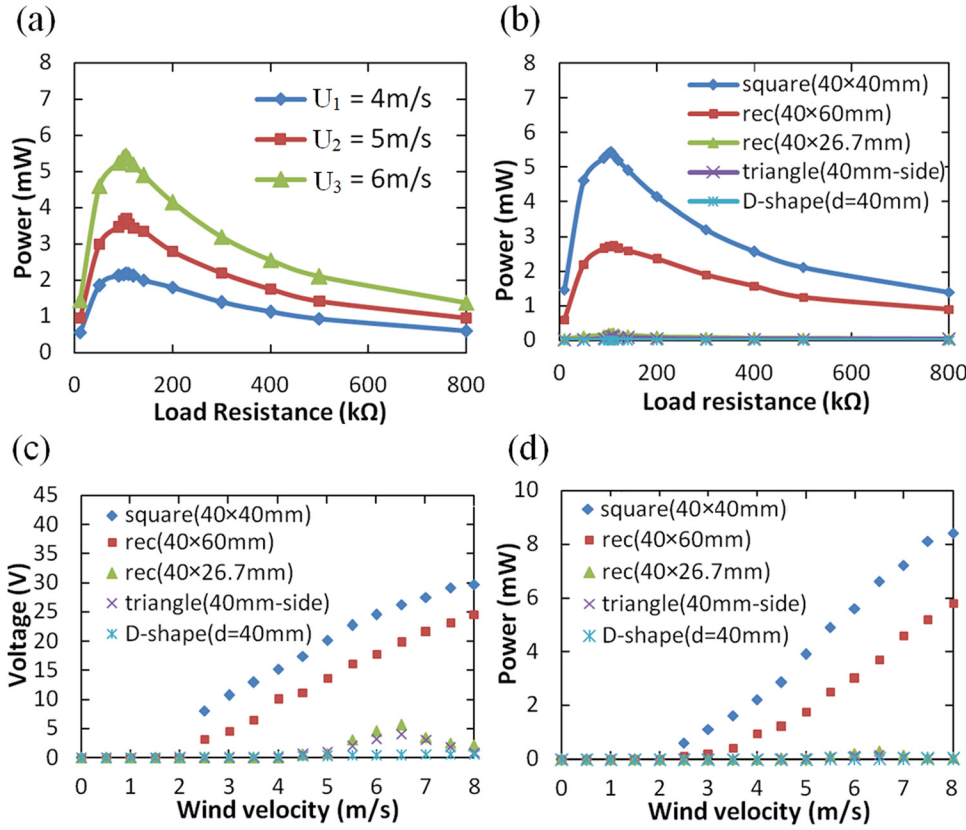
FIG. 3. Experimental results for various cross sections: (a) Power versus load resistance for square-section tipped energy harvester; (b) power versus load resistance at 6 m/s; (c) voltage versus wind velocity at 105 kΩ; (d) power versus wind velocity at 105 kΩ.

rectangle (40×26.7 mm^2), D-section, and equilateral triangle are quite low. The reason for the first two sections is the failure to meet the criterion of galloping instability in the laminar flow (which is the case for our test), as $\partial C_{Fz}/\partial \alpha$ equals to 0 for the rectangle (40×26.7 mm^2) and -0.1 for the D-section, respectively.[24] However, in the turbulent flow, the value for the D-section becomes positive (i.e., $\partial C_{Fz}/\partial \alpha = 0.79$ for turbulence intensity Tu = 11%), which enables the D-section to undergo self-excited oscillation as presented by Sirohi and Mahadik.[21] They blew the D-section with an axial fan that generated turbulent flow and obtained a stable output power around a wind velocity of 5.5 mph. For equilateral triangle, the predicted cut-in wind velocity is around 8.5 m/s, which is beyond our testing range. The minor peaks for the rectangle (40×26.7 mm^2) and equilateral triangle are caused by the resonance at the first torsional mode due to the vortex shedding (Figures 3(c) and 3(d)). Slight irregular torsional deflections were observed during the wind tunnel test when the wind velocity reached 5.5 m/s. These deflections increased to the maximum (resonance) at 6.5 m/s and then disappeared over 7.5 m/s, as the vortex shedding frequency increased with the wind velocity.

The responses of the harvester with preferred square-sectioned tip can be predicted by simulation with the derived analytical model. The short circuit and open circuit natural frequencies for the proposed harvester are measured to be 6.84 Hz and 6.89 Hz under base excitations, respectively. The electromechanical coupling coefficient Θ is then determined to be 0.000373 N/V by Eq. (2). The damping ratio ζ, which is expressed as $\zeta = C/(2M_{eff}\omega_{nsc})$, is measured using the logarithmic decrement technique. The harvester is first excited at 6.84 Hz at the unity RMS acceleration and then

the shaker is suddenly shut down to obtain the attenuation curves of short circuit current, from which ζ is calculated to be 0.0148. The coefficients A_i and A_j for square cross section are shown in Table II.[24]

Using the above parameters, the output power versus wind velocity is calculated by numerical integration (Fig. 4(a)). Obvious discrepancy between the calculated and measured power is observed. This should be attributed to the inaccurate damping ratio used in the simulation. In practice, the damping is amplitude-dependant, i.e., not constant. When the energy harvester is subjected to the low-speed wind flow in our test, the oscillation amplitude is much smaller than that in the logarithmic decrement test. For a more rational simulation, after a few trials, a modified damping ratio of 0.005 is used for the voltage and power prediction. The calculated output power versus load resistance agrees well with the measured results as shown in Fig. 4(b). The calculated voltage and output power at 105 kΩ are plotted in Figs. 4(c) and 4(d), respectively. Again, the results match well with the measured data except for the hysteresis region between 2.8 m/s and 3.8 m/s. Theoretically, when wind velocity increases from zero to 3.8 m/s, the power should increase along line 1, then jump to the upper line 2 increasing along it till 8 m/s. When the wind velocity reduces from 8 m/s to 2.8 m/s, the power should decrease along line 2, and then drop to line 1 at 2.8 m/s. However, the experiment does not

TABLE II. Aerodynamic coefficients of polynomial expansion of C_{Fz}.

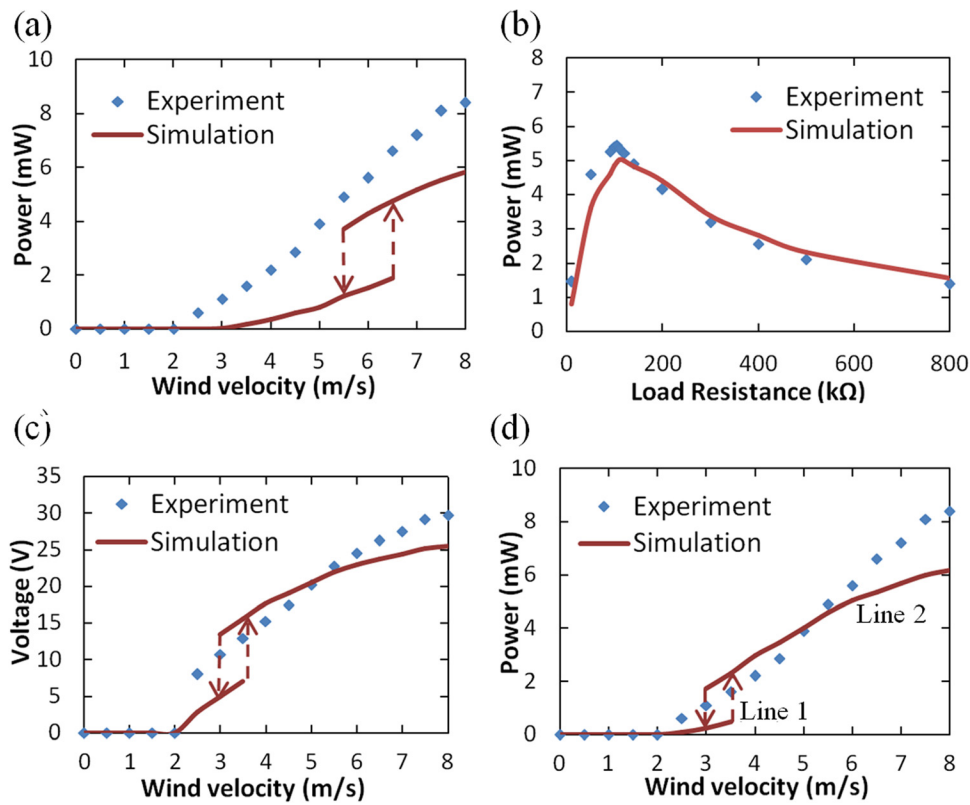| Coef.	A_1	A_2	A_3	A_4	A_5	A_6	A_7
Square	2.69	0	1.684×10^2	0	6.27×10^3	0	5.99×10^4

FIG. 4. Simulation results for square section: (a) Power versus wind velocity at 105 kΩ; (b) power versus load resistance at 6 m/s; (c) voltage versus wind velocity at 105 kΩ; (d) power versus wind velocity at 105 kΩ. (a) Use the initial ζ, (b)–(d) use the modified ζ.

capture this hysteresis phenomenon. Sources for these discrepancies may include the use of constant damping in simulation, the vortex shedding from the tip body, and the difference between the operating condition such as Reynolds number in our test and that used in Ref. 24 to get the aerodynamic coefficients.

In summary, this letter presents a comparative study of galloping energy harvester with different cross-section tips. Experimental results confirm the superiority of square cross-section tip over the others used in the literature. A peak output power of 8.4 mW is achieved which is sufficient to power small sensors. An analytical model is established and verified by experimental results. It is recommended that the tip of square section should be used for galloping-based small wind energy harvesting.

[1]S. R. Anton and H. A. Sodano, Smart Mater. Struct. **16**, R1 (2007).
[2]A. Erturk and D. J. Inman, Smart Mater. Struct. **17**, 065016 (2008).
[3]Y. W. Yang, L. H. Tang, and H. Y. Li, Smart Mater. Struct. **18**, 115025 (2009).
[4]L. H. Tang, Y. W. Yang, and C. K. Soh, J. Intell. Mater. Syst. Struct. **21**, 1867 (2010).
[5]I. H. Kim, H. J. Jung, B. M. Lee, and S. J. Jang, Appl. Phys. Lett. **98**, 214102 (2011).
[6]S. G. Li, J. P. Yuan, and H. Lipson, J. Appl. Phys. **109**, 026104 (2011).
[7]M. Bryant and E. Garcia, Trans. ASME, J. Vib. Acoust. **133**, 011010 (2011).
[8]A. Erturk, W. G. R. Vieira, C. De Marqui, Jr., and D. J. Inman, Appl. Phys. Lett. **96**, 184103 (2010).
[9]A. Abdelkefi, A. H. Nayfeh, and M. R. Hajj, Nonlinear Dyn. **68**, 531 (2012).
[10]A. Abdelkefi, M. R. Hajj, and A. H. Nayfeh, J. Intell. Mater. Syst. Struct. **23**, 1523 (2012).
[11]S. D. Kwon, Appl. Phys. Lett. **97**, 164102 (2010).
[12]H. Liu, S. Zhang, R. Kathiresan, and T. Kobayashi, Appl. Phys. Lett. **100**, 223905 (2012).
[13]H. D. Akaydin, N. Elvin, and Y. Andreopoulos, Smart Mater. Struct. **21**, 025007 (2012).
[14]V. Sivadas and A. M. Wickenheiser, Proc. SPIE **7977**, 79770F (2011).
[15]L. A. Weinstein, M. R. Cacan, P. M. So, and P. K. Wright, Smart Mater. Struct. **21**, 045003 (2012).
[16]H. J. Jung and S. W. Lee, Smart Mater. Struct. **20**, 055022 (2011).
[17]N. G. Elvin and A. A. Elvin, J. Intell. Mater. Syst. Struct. **20**, 2017 (2009).
[18]A. Bibo, G. Li, and M. F. Daqaq, J. Intell. Mater. Syst. Struct. **23**, 1461 (2012).
[19]A. Barrero-Gil, G. Alonso, and A. Sanz-Andres, J. Sound Vib. **329**, 2873 (2010).
[20]J. Sirohi and R. Mahadik, J. Intell. Mater. Syst. Struct. **22**, 2215 (2011).
[21]J. Sirohi and R. Mahadik, Trans. ASME, J. Vib. Acoust. **134**, 011009 (2012).
[22]A. Abdelkefi, M. R. Hajj, and A. H. Nayfeh, Smart Mater. Struct. **22**, 015014 (2013).
[23]J. P. Den Hartog, *Mechanical Vibrations* (McGraw-Hill, New York, 1956).
[24]M. P. Païdoussis, S. J. Price, and E. de Langre, *Fluid-Structure Interactions: Cross-Flow-Induced Instabilities* (Cambridge University Press, 2011).